



HAL
open science

Physical and chemical characteristics of particles emitted by a passenger vehicle at the tire-road contact

Asma Beji, Karine Deboudt, Bogdan Muresan, Salah Khardi, Pascal Flament, Laurence Lumiere, Marc Fourmentin

► To cite this version:

Asma Beji, Karine Deboudt, Bogdan Muresan, Salah Khardi, Pascal Flament, et al.. Physical and chemical characteristics of particles emitted by a passenger vehicle at the tire-road contact. Chemosphere, 2023, 340, pp.139874. 10.1016/j.chemosphere.2023.139874 . hal-04205389

HAL Id: hal-04205389

<https://ulco.hal.science/hal-04205389>

Submitted on 12 Sep 2023

HAL is a multi-disciplinary open access archive for the deposit and dissemination of scientific research documents, whether they are published or not. The documents may come from teaching and research institutions in France or abroad, or from public or private research centers.

L'archive ouverte pluridisciplinaire **HAL**, est destinée au dépôt et à la diffusion de documents scientifiques de niveau recherche, publiés ou non, émanant des établissements d'enseignement et de recherche français ou étrangers, des laboratoires publics ou privés.



Distributed under a Creative Commons Attribution - NonCommercial - NoDerivatives 4.0 International License

Physical and Chemical Characteristics of Particles Emitted by a Passenger Vehicle at the Tire-Road Contact

Asma BEJI^{1,2}, Karine DEBOUDT^{1*}, Bogdan MURESAN², Salah KHARDI³, Pascal FLAMENT¹,
Marc FOURMENTIN¹, Laurence LUMIERE²

¹Laboratory of Physics and Chemistry of the Atmosphere (LPCA), Université du Littoral Côte d'Opale (ULCO), 59140 Dunkerque, France.

²Environment-Planning, Safety and Eco-design (EASE-AME) Laboratory, Gustave Eiffel University, 77454 Marne-la-Vallée, France.

³University of Lyon, CNRS, INSA Lyon, LaMCoS, UMR 5259, 69621 Villeurbanne, France

*: Corresponding author

Email: karine.deboudt@univ-littoral.fr

Mailing address: 189A avenue Maurice Schumann, 59140 Dunkerque, France (EU)

Phone: +33(0)3 2823 7631

Keywords (6 max): non-exhaust emission, tire-road wear particles, road dust, individual particle composition, SEM-EDX

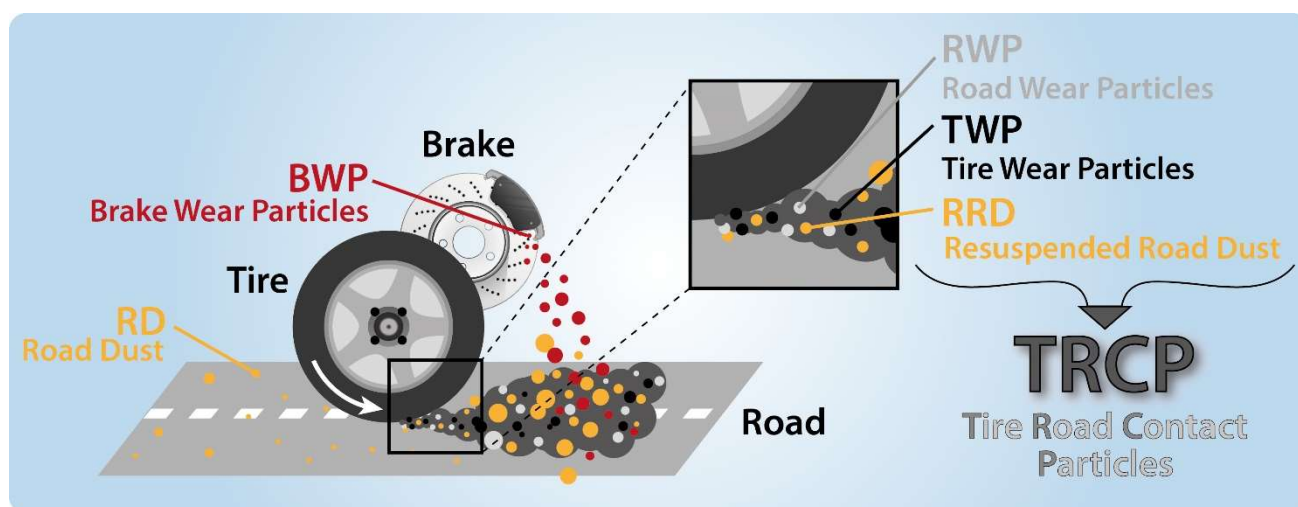
Highlights:

- Tire Road Contact Particles (TRCP) can be classified according to their chemical composition to identify their origins
- Brake wear particles are Fe-rich particles and also contain tracers such as Ba or Mn
- Tire wear particles are carbonaceous particles containing Si, Zn, and S
- Mineral incrustation, from road wear/dust, are often embedded in the tire tread
- At the individual particle scale, TRCP are mostly contaminated by road dust

28 **Abstract:**

29 Non-exhaust emissions are now recognized as a significant source of atmospheric particulate matter
30 and the trend towards a reduction of conventionally fueled internal combustion engine vehicles on the
31 road is increasing their contribution to air pollution due to lower exhaust emissions. These particles
32 include brake wear particles (BWP) and tire-road contact particles (TRCP), which are composed of
33 tire wear particles (TWP), road wear particles (RWP) and resuspended road dust (RRD). The goal of
34 this study has therefore been to design an original experimental approach to provide insight into the
35 chemical composition of particles emitted at the tire-road contact, focusing on the micron ($PM_{10-1\mu m}$)
36 and submicron ($PM_{1-0.1\mu m}$) fractions. Through this characterization, an examination of the different
37 TRCP generated by different materials (tire, road surface, brake system) was conducted. To achieve
38 this, TRCP were collected at the rear of the wheel of an instrumented vehicle during road and track
39 tests, and a SEM-EDX analysis was performed. Our experimental conditions have allowed us to
40 demonstrate that, at the individual particle scale, TRCP are consistently associated with road dust
41 materials and particles solely composed of tire or road materials are practically non-existent. The
42 contribution of BWP to TRCP is marked by the emission of Fe-rich particles, including heavy metals
43 like Ba, Mn and Cr. TWP, which result from rubber abrasion, consist of C-rich particles abundant in
44 Si, Zn, and S. RWP, mainly composed of Al, Si, Fe, and Ca, can be either part of RRD or internally
45 mixed with emitted TWP. The findings of this study highlight the substantial role of RRD to TRCP
46 emissions under real driving conditions. Consequently, it underscores the importance of examining
47 them simultaneously to achieve a more accurate estimation of on-road traffic emissions beyond the
48 vehicle exhaust.

49
50 **Graphical abstract:**



51

52

53 1. Introduction..... - 4 -

54 2. Materials and Methods..... - 7 -

55 3. Results and Discussion - 10 -

56 3.1. Source materials - 10 -

57 Tire and tire wear particles (TWP) - 10 -

58 Brake system and brake wear particles (BWP)..... - 11 -

59 3.2. Source and characterization of Tire Road Contact Particles (TRCP)..... - 13 -

60 Super-coarse TRCP..... - 13 -

61 Micron and submicron TRCP in real-driving conditions - 15 -

62 Micron and submicron TRCP emissions in the absence of road salting..... - 16 -

63 4. Conclusion - 17 -

64 6. References..... - 19 -

65 List of Table..... - 25 -

66 Figure Captions..... - 26 -

67 Figure 1 - 28 -

68 Figure 2 - 29 -

69 Figure 3 - 30 -

70 Figure 4..... - 31 -

71 Figure 5 - 32 -

72 Figure 6 - 33 -

73

74 **1. Introduction**

75 Contribution of atmospheric Particulate Matter (PM) to urban air pollution has been a rising
76 concern throughout the world in recent years. Non-exhaust traffic-related sources are now
77 acknowledged as a major contributor to PM, that may account for ≈ 66 wt.% of the coarse PM fraction
78 ($PM_{10-2.5}$) and ≈ 29 wt.% of the fine PM fraction ($PM_{2.5-0.2}$), in the urban atmosphere (Matthaios et
79 al., 2022). Both fine and coarse PM fractions coming from non-exhaust emissions include brake wear,
80 tire and -road wear, and resuspension of road dust (Fussell et al., 2022). Many studies have focused on
81 non-exhaust particles (NEP) and their composition (Harrison et al., 2021) and references therein. As
82 illustrated by Figure 1, NEP include brake wear particles (BWP), a fraction of resuspended road dust
83 (RRD) and tire-road contact particles (TRCP). TRCP include tire wear particles (TWP) and road wear
84 particles (RWP), as well as some RRD. The latter can initially come from road use, vehicles, or other
85 sources, as terrigenous particles (mineral dust) resuspension. TRCP emissions are likely to change as
86 a result of many factors, mainly weather and traffic conditions, friction forces, tire types and road
87 surface characteristics (Matthaios et al., 2022; Yan et al., 2021; Youn et al., 2021). In order to better
88 constrain these emissions and limit their environmental and health impact, it is essential to assess the
89 relative proportion of the different possible origins (notably TWP, RWP or RRD) in real-world
90 conditions and better understand their physical and chemical properties, which is the aim of the present
91 study.

92 In scientific literature, the terms “tire wear particles (TWP)” and “Tire and road wear particles
93 (TRWP)” are often used even if what is meant is TRCP, including RRD. Therefore, difficulties arise
94 when studying TRCP due to a lack of standardized sampling procedures and measurement techniques,
95 which leads to non-comparable results (Mattonai et al., 2022; Piscitello et al., 2021; Zhang et al., 2023).
96 In most previous studies, TRCP measurements and sampling have been conducted without attempting
97 to differentiate between each source contribution (tire wear, road wear or resuspension road dust), but
98 by considering TRCP as a complex mixture of diverse particles. Many studies have focused on TWP

99 emissions, generally using tire simulators (Cao et al., 2022), or on RWP (Baensch-Baltruschat et al.,
100 2020; Gustafsson, 2018), while those specifically targeting TRCP emissions (including TWP, RWP
101 and RRD) are relatively rare, due to the high contribution of RRD, which make the situation much
102 more complex for measurement and sampling methodologies (Harrison et al., 2021). In a companion
103 study (Beji et al., 2021) based on emission dynamics and size distribution observed during road and
104 track measurements, tire and road wear particles were found to make up an average of 40% of the rear-
105 of-wheel particles' (here called TRCP) direct contribution. The results depended on road surface
106 contamination, road surface texture, driving area, and structural elements affecting road traffic. TWP
107 were found to have varied morphologies (elongated, round, irregular, etc.) and wide-ranging elemental
108 compositions, although they differ in physical and chemical properties from the original tire material
109 (Wagner et al., 2018). The ultrafine fraction generated from the tire tread is generally marked by high
110 carbonaceous content associated with silicon and sulfur (Park et al., 2018). Mineral-rich particles from
111 TRCP, mostly in the fine fraction, are generally incrustated within rubber particles (Adachi and
112 Tainosho, 2004; Alves et al., 2020; Rausch et al., 2022) and are mainly produced by road surface
113 abrasion (Celo et al., 2021; Cunha-Lopes et al., 2022). The dominating mineral content of road wear
114 particles is due to the composition of rock aggregates and other mineral fillers such as fly ash particles
115 (Chen et al., 2022) incorporated into the asphalt mix to enable desired performance (Chousidis et al.,
116 2016; Kim et al., 2020; Xu and Shi, 2018). All of these materials can disintegrate from the road surface
117 and form RWP, which become part of the road dust, can be re-suspended and then included in
118 Resuspended Road Dust (RRD), a major source of particles in TRCP. Road dusts are essentially
119 composed of minerals, but also tire and bitumen wear particles (Gao et al., 2022; Järllskog et al., 2022).
120 Giant road dusts generally contain a high amount of elongated particles resulting from tire abrasion,
121 while the micrometric and submicrometric fractions contain a higher amount of angular mineral-
122 containing particles. These mineral-containing particles potentially come from surrounded soil, but
123 also from road traffic (brake, tire and road wear), the latter being notably characterized by the presence

124 of C, Al, Si, Ti, S, Ca, Fe and Zn (Gunawardana et al., 2012). Road dusts also contain spherical
125 particles with smooth surfaces, which may be fly ash from asphalt (Mistry and Roy, 2016). Several
126 studies have also identified heavy metals from previously deposited non-exhaust particles present in
127 road dust (Candeias et al., 2020; Padoan et al., 2017). In particular, Fe exhibits the highest
128 concentration of metals in the fine fraction, which may originate from brake wear (Yang et al., 2016;
129 Zhang et al., 2020). BWP contribution to TRCP is limited during normal driving and acceleration
130 conditions, but it has to be accounted during heavy braking situations (Beji et al., 2020, Mathissen et
131 al., 2011). Once deposited on the road surface, BWP can be weathered and incorporated into the
132 resuspended dust cloud, thus falling into the category of RRD, as previously deposited TWP and RWP.
133 Therefore, both their chemical composition and morphology can be altered compared to freshly
134 emitted BWP. The chemical composition of brake systems can provide valuable insight into the origin
135 and formation processes of BWP. In most cases, the disc is made of gray cast iron. The brake pads
136 have far more complex components, which vary considerably depending on the local market and
137 manufacturers (Harrison et al., 2021). Fe is ubiquitous in both TWP and RWP and therefore cannot be
138 considered exclusive of BWP emissions. However, some associated chemical elements are considered
139 to be common tracers of brake wear, including Cu and Ba (Fussell et al., 2022; Harrison et al., 2021;
140 Charron et al., 2019; Sanders et al., 2003).

141 The aim of this study has therefore been to determine the probable origin of TRCP (i.e. brake
142 wear, tire wear, road wear and/or road dust resuspension) based on their size range and chemical
143 composition. Considering their significant impact on human health, we have focused more particularly
144 on micrometric and submicrometric particles. To do this, we investigated the chemical composition of
145 source materials (tire, road surface and brake pads) and the physical/chemical components of TRCP
146 emissions collected in real-world using an instrumented vehicle. Individual particle analysis using
147 automated scanning electron microscopy (SEM) coupled with energy dispersive X-ray spectroscopy

148 (EDX) has been used to analyze the particles collected during on-road and on-test track experiments.
149 This paper evaluates the significance of the road dust as a contributor of TRCP emissions.

150

151 **2. Materials and Methods**

152 Test-track and on-road measurement campaigns have been described in detail elsewhere (Beji
153 et al., 2021). In summary, on-board measurements were carried out in two different environments: a
154 2.3 km test track with a maximum speed of 140 km/h (semi-controlled environment) and on the road
155 (real-driving conditions). The travelled route was a 25-km long loop in the Nantes metropolitan area
156 (northwestern France), passing through different environments (rural, urban and motorways) and
157 covering several road types (country roads, ring roads, city streets, etc.), with the aim of providing
158 variable RRD, both in quantity and type. On-board measurements were conducted on the test track and
159 on the road under the same weather conditions (wind speed below 7 m.s⁻¹, no rain in seven days before
160 the experiments, temperature ranges from 20 °C to 25 °C, and humidity ranges from 50% to 80%).
161 The road surface of the test track was a semi-coarse asphalt concrete with medium macrotexture and
162 microtexture levels. The constituent rocks, originally from local quarries, were composed
163 predominantly of quartz and feldspars, containing the same elements as granite (O, Si, Al, Na, K and
164 to a lesser degree Fe, Ca and Mg), but in slightly different proportions. As the test track was subject to
165 limited traffic and was regularly cleaned of ambient dust deposition and particle emissions from
166 previous tests, road dust contamination level was expected to be higher on the Nantes metropolitan
167 area roads. This strategy aimed to analyze various components contributing to TRCP by examining
168 source materials (tire, pavement, brake system, etc.).

169 The experiments were performed with a fully-equipped vehicle (Renault Clio 3, one of the most
170 common models sold in France), fitted with commercial summer tires (MichelinTM Energy Saver,
171 185/60 R 15 88H) and semi-metallic brake pads (TRW 8200). A trailer containing the scientific

172 instrumentation was hitched to the car (Figure 2). The same vehicle was used for all measurements,
173 and tests were conducted by the same driver and co-driver to preserve the same driving behavior
174 throughout the experiments. The tests provided insight into several dynamics parameters (driving
175 speed variations, fuel consumption, brake pressure, etc.) and particle size distributions (aerodynamic
176 diameters ranging between 7 nm and 10 μm) in real-time. More details about the devices used and
177 particles sizing results are reported in Beji et al. (2021). Although variable over time, the proportion
178 of particles from the atmospheric background (measured when the vehicle is stationary) was relatively
179 low, reaching a maximum of 5% and 28 % for on-road and test track experiments, respectively (Beji
180 et al. 2021). The amount of resuspended road dust was lower on the cleaned test track, resulting in this
181 relatively greater contribution of the atmospheric background. At the end of the experiments, brake
182 pads and tires were dismantled in order to study them by microscopy. The used surfaces of the brake
183 pad and of the tire tread zone were thus observed and compared with unused surfaces obtained by
184 fracture. For that, a piece on the surface of the pad is broken off and a piece of the surface of the tire
185 previously soaked in liquid nitrogen is torn off.

186 A three-stages cascade impactor (air flow: 28 $\text{L}\cdot\text{min}^{-1}$) with nominal cut-off diameters (i.e.
187 aerodynamic diameter at 50% of collection efficiency) of 10, 1.0 and 0.1 μm was used for particle
188 sampling. Particles were collected on nickel Transmission Electron Microscopy (TEM) grids, attached
189 to polycarbonate membranes. The air inlets for particle collections were placed at the rear of the front
190 tire (driver side) and in the backspace of the wheel near the braking system (Figure 2). The inlet of
191 tire-road contact particles sampling probe was set 15 cm behind the tire and 7 cm above the ground,
192 the best position to sample TRCP from both tire-road wear and the resuspension of road dust induced
193 by vehicle turbulence. Moreover, the instrument's calculated aspiration efficiencies (η) approached
194 100% for particles smaller than 10 μm , irrespective of the vehicle speed (Beji et al., 2021). Potential
195 contamination by fresh brake wear particles emissions was also assessed by simultaneously sampling
196 at the rear and in the backspace of the instrumented wheel (i.e. 15 cm below and 12 cm downstream

197 of the braking system). As a result, it became feasible to examine the chemical composition of brake
198 wear particle emissions and distinguish them among TRCP emissions. For super-coarse particles
199 (diameter larger than 10 μm), passive sampling on carbon adhesive attached at the end of the air inlet
200 was used (Figure 2).

201 Individual particle analyses were performed by automated Scanning Electron Microscopy with
202 Energy-Dispersive X-ray spectrometry acquisition (SEM-EDX). The assumption is that super-coarse
203 particles with highly agglomerated shapes come from various sources, so about a hundred particles
204 have been analyzed manually to gain further insight into the chemical composition and texture of the
205 different agglomerate fragments. This type of analysis is useful but time-consuming, so not suitable
206 for studying a large volume of particles. For micron- and submicron-sized particles (with diameter <
207 10 μm), automated analysis detected several hundred particles per impactation stage. The SEM-EDX
208 used is a JEOL 7100F FEG-SEM, equipped with a transmitted electron detector and three ultrathin-
209 window (30 mm^2) energy-dispersive X-ray detectors (Bruker XFlash 6/30). Spectral acquisitions were
210 performed at 15 kV, 300 pA for 20 s. The EDX spectrometers were calibrated before analyses using
211 the Cu $K\alpha$ -line at 8041 eV. The elemental concentrations were calculated using the PhiRoZ
212 quantification procedure from Esprit Software (Bruker Nano, Germany). Particles smaller than 100
213 nm were not considered because they do not produce a sufficient X-ray signal to obtain a reliable EDX
214 spectrum. There are various ways of processing data from individual particle analysis, ranging from
215 manual particle classification to elaborate classifications using machine learning (Rausch et al., 2022).
216 In our case, the resulting large databases (elemental compositions in weighted %, and particle size)
217 were statistically analyzed by means of Hierarchical Ascending Classification (HCA), using the
218 FactoMineR[®] software, clustering particles with similar elemental compositions, so probably from the
219 same source. The particles are then sorted by sample and each cluster of a sample is assigned to a
220 particle family among seven families (Table 1, from A to G) based on its mean elemental composition.
221 If several clusters of a same sample were assigned to the same family (due, for example, to a variable

222 proportion of an element of no interest such as Na), these clusters were grouped together to form a
223 single cluster. Finally, the sum of the spectra was calculated for each cluster of a sample to improve
224 the signal to noise ratio and deduce an accurate average elemental composition of particles classified
225 in this cluster.

226 **3. Results and Discussion**

227 **3.1. Source materials**

228 Tire and tire wear particles (TWP): In our study, a summer silica-based tire was used. These tires have
229 asymmetrical structures with three straight grooves that run around the center of the rubber tread. The
230 chemical mapping of the unused tread zone, which has never been in contact with the road, is mainly
231 composed of Si, C and O with, to a lesser extent, S and Zn, in accordance with literature data
232 (Supporting Information, Figure S1A). The high Si content of the tire tread is due to the use of
233 amorphous silica in filler materials with black carbon, to enhance the mechanical and dynamic
234 properties of rubber (Rattanasom et al., 2007). In contrast, the chemical mapping of a tread zone after
235 used (subsequent to contact with the road surface) has a heterogeneous chemical composition with a
236 larger number of detected elements (C, O, Si, Al, S, Na, Mg, K, Ca, Fe, Zn, Ti) (Supporting
237 Information, Figure S1B). With the exception of Fe and Ti, all of these mineral components were
238 previously reported by Kovoichich et al. (2021) using SEM-EDX mapping of super-coarse particles
239 coming from three used tread surfaces. Mineral incrustations were also observed at the tire tread
240 surface (Figure S1B). These may come from road wear or resuspended mineral dust. When a tire comes
241 into contact with the road, some road dust is collected onto the tire surface before being stripped off
242 and carried away by air flow. Furthermore, a portion of the particles may undergo crushing between
243 the road and the tire tread surface, leading to potential alterations in the physical and chemical
244 properties of emitted particles. These changes may differentiate them from road dust that has only
245 recently settled on the tread surface and become part of the TRCP fraction.

246 Mineral incrustations found on asphalt pavement can exhibit varying contents of Al, Si, Fe, K,
247 Ca and Mn, which can be attributed to the use of steel slag, limestone and manganese dioxide as fillers
248 to improve mechanical performances of asphalt, facilitating self-healing capabilities (Deng et al., 2022;
249 Wei et al., 2021). In addition to particles coming from mineral incrustations of road surface, the tire
250 tread surface may generate both coarse elongated particles (micrometer-scale) and irregular
251 submicrometer TWP, with a more or less rounded shape (Kim and Lee, 2018). While the large
252 elongated particles are formed mechanically by shear and friction forces in the slip between tire and
253 the road, the fine TWP can be emitted by volatilization processes due to frictional heat under severe
254 conditions (Baensch-Baltruschat et al., 2020; Park et al., 2017). For Sommer et al. (2018), “pure”
255 super-coarse TWP exist only in very low quantities in the environment and TWP are quickly mixed
256 with RWP and BWP in high traffic roads (Eisentraut et al., 2018). The resulting mixture contains heavy
257 metals such as Zn, Fe, Ba, Cu and Sb, in addition to Si and Ca coming from RWP. Al is ubiquitous: It
258 is present in clayey background dust, asphalt pavement, as well as in rubber additives and brake
259 abrasion particles (Sommer et al., 2018). In summary, the interaction of the tire tread with the road
260 could generates various TWP through mechanical and also thermal mechanisms. These particles can
261 originate from the degradation of the tire materials, but also from road dust previously stuck on the
262 surface of the tread. However, frictional interaction can change both the chemical properties and the
263 morphologies of TWP compared to the original tread materials and the deposited road dust.

264 Brake system and brake wear particles (BWP): The brake system used in our on-board measurements
265 was a semi-metallic brake lining with a cast iron disc. Elemental maps of an unused surface of the
266 brake pad have underlined the heterogeneous elemental distribution at the micrometric scale
267 (Supporting Information, Figure S2). Some areas have Fe-rich components, while others are mainly
268 composed of carbonaceous materials or mixed carbonaceous/metal agglomerates (containing notably
269 C, O, Al, Si, S, Fe and Mg). This heterogenous elemental distribution within the pad will generate,
270 upon thermal process and/or mechanical degradation, various chemical compositions of BWP.

271 Moreover, during braking, friction materials from this pad and the disc act as contributor and
272 nucleation sites for the formation of the third body inside the friction layer (Kukutschová et al., 2009).
273 This third body is a complex and discontinuous layer of very fine wear particles that are pressed and
274 sintered together. It has its own chemistry and microstructure which differ from the microstructure and
275 chemistry of the phases present in the original bulk materials. Its formation and disruption greatly
276 influence particle emission dynamics since it accounts for a large proportion of the released wear
277 particles (Gomes Nogueira et al., 2020). Thus, the characteristics of emitted particles (size, shape,
278 chemistry) are highly variable according to the friction material composition itself, and BWP generated
279 from the third body may have a different composition than those of the discs and pads.

280 Particle sampling near the brake system during the on-board experiment on the test track (Figure 2)
281 allowed us to characterize the instrumented car BWP and thereby evaluate their contribution to the
282 composition of TRCP. Even if the sampling was performed continuously during the trip (during
283 braking and non-braking), the position of the air inlet allowed us to collect chiefly BWP (Beji et al.,
284 2021). Collected BWP have various morphological properties and sizes (Supporting information,
285 Figure S3): spherical, irregular and agglomerated particles. Micron-sized BWP were often
286 agglomerated in shape, whereas submicron-sized BWP tended to be spherical or irregular.

287 The same air inlet implementation (backspace of the wheel) was used during real driving (i.e., “on
288 road”) experiments to determine the chemical makeup of BWP. Based on their elemental composition
289 (except C and O, which may come from the collection substrate), particles collected near the braking
290 system during the on-road experiment were statistically classified by the HCA technique into different
291 clusters (Figure 3), according to their size (micron [1-10 μ m] and submicron [0.1-1 μ m] fractions). The
292 sum of the relative contribution (RC) of two first clusters (#1 and #2) represent around 90% of analyzed
293 particles for the two fractions. For these clusters (except R-BWP-S2), 32 to 61wt.% of analyzed
294 particles are Fe-rich (Fig.3). With the exception of Cu, the consistent presence of Ba, Cr, Mn, Ti and
295 Zn strongly suggests that these particles are directly emitted from brake pads and/or discs. Therefore,

296 they can be regarded as freshly emitted BWP (Fussell et al., 2022; Harrison et al., 2021). Occasionally,
297 Na, Cl and N were detected (≤ 10 wt.%). Because the last road salting in the area took place three weeks
298 earlier, we hypothesize that these components probably come from road salt previously deposited as a
299 de-icing agent, even if light rainfall subsequent to the salting (4.4 mm/day on average and never more
300 than 18.7 mm/day) did occur. Despite the position of the air inlet as close as possible to the braking
301 system (Fig. 2), the collection of RRD cannot be excluded. Indeed, the collection of particles was
302 maintained throughout the on-road experiment and particles were inevitably collected in the absence
303 of braking. Nevertheless, the monitoring of particle concentrations at the sampling point indicated that
304 the relative proportion of these particles (probably RRD) was low when they were integrated over the
305 entire duration of the on-road experiment. In fact, it is worth noting that the ubiquitous elements in
306 road dust (Al, Si, Ca and S) were mainly (but not only) detected in minority clusters (M3, M4, and M5
307 for the 1-10 μ m fraction and S3 and S4 for the 0.1-1 μ m fraction).

308 To sum up, the particles collected near the brake system during on-road experiments consist of both
309 freshly emitted BWP generated during friction processes and some RRD containing elements like Na,
310 N or Cl. Apart from C and O, Fe is the primary element identified in BWP during both test track and
311 on-road experiments, often found in internally mixed particles with minor elements such as Mn, Ba,
312 Cr, Ti and Zn. While Fe is widespread in all wear particles (TWP, RWP and BWP), the recurrent
313 presence of Mn and Ba in the main groups of particles analyzed make them valuable as specific tracers
314 of BWP emissions.

315

316 ***3.2. Source and characterization of Tire Road Contact Particles (TRCP)***

317 Super-coarse TRCP: Super-coarse particles are defined in this study as particles with a diameter > 10
318 μ m. Figure 4 shows representative pictures of super-coarse TRCP collected at the *rear of the wheel*
319 during the test-track experiment (Fig.2). They often have an elongated or irregular shape and are

320 composed of various elements such as: C, O, Si, Al, S, Fe, Ca, Na, K, Mg, Mn, and Cr. The particle
321 presented in Figure 4(a) is mineral-rich, having an irregularly shape with a rough surface, probably
322 coming from road abrasion. Figure 4(b) shows particles with an elongated shape, typical of TWP
323 (Gunawardana et al., 2012; Kovoichich et al., 2021; Park et al., 2018; Sommer et al., 2018). Figures
324 4(c) and (d) are carbon-rich particles, with an irregular shape and containing mainly Ca, Si and S,
325 which suggests that they are probably from tire tread abrasion: Black carbon, silica and chalk are used
326 as reinforcing fillers in tire materials, while S is a vulcanization agent (Kovoichich et al., 2021). Figure
327 4(d) shows Si- and Ca-rich particles, which strongly suggest that they likely originate from the filler
328 mixture of the tire tread or from road abrasion. In contrast, the image in 4(e) shows a carbonaceous
329 particle without mineral elements, which means that it is likely TWP coming from the rubber part of
330 the tread. The “E” area of Fig.4(e) has a flaked shape at high magnification, likely coming from the
331 tire rubber peeling (Camatini et al., 2001). Another common type of super-coarse TRCP involves the
332 presence of agglomerated particles, which are likely from diverse sources (Figure 4-f, “F” areas
333 images). These agglomerates are made of incrustations of mineral particles (F1) into a rubber fragment
334 (F2). We assume that the flaked-shape surface of rubber particles offers a large contact zone, which
335 promotes the inclusion of RWP into the rubber fraction of TWP (Knight et al., 2020; Kreider et al.,
336 2010). Sommer et al. (2018) also observed the presence of agglomerated TWP and RWP in
337 atmospheric super-coarse particles collected near highways.

338 According to their morphology and elemental composition, super-coarse TRCP exhibit distinct
339 origins and can be classified into three categories. RWP, which exhibit a high-mineral content
340 (typically including Al, Si, Fe and Ca) and an irregular shape, characteristic of road abrasion. Carbon-
341 and metal-rich TWP that come from the wear of the tire rubber, including the filler mixture of the tire
342 tread. This second category features an elongated shape that is more or less irregular and presents a
343 rough surface. Lastly, agglomerated particles, which presumably consist of mineral incrustations
344 embedded in tire rubber, i.e., an external mixture of TWP and RWP or RRD. These super-coarse

345 particles mainly reflect the mechanical abrasion of tire tread and/or road surface, as well as the
346 subsequent agglomeration processes. Although they can be resuspended by the passage of vehicles,
347 they probably do not have a significant impact on air quality considering their rapid sedimentation,
348 due to their size. Nevertheless, after undergoing sedimentation and possible fragmentation, these
349 super-coarse TRCP could serve as persistent sources of particulate pollutants and may release
350 leachable metallic/organic compounds to roadside soils or to aquatic environments.

351 Micron and submicron TRCP in real-driving conditions: The micron and submicron fractions of the
352 collected TRCP were of significant interest due to their presence in the respirable size range and direct
353 link to a number of human diseases (Halle et al., 2020; Kreider et al., 2020). Figure 5 shows the HCA
354 clusters for TRCP sampled during the on-road measurements according to their size fraction and
355 chemical composition. The likely origin of these particles was determined by comparing their
356 composition with that of the source materials, enabling the classification of each cluster into one of
357 the seven families of particles (from A to G, Table 1). Particles from clusters R-TRCP-M3 and R-
358 TRCP-S2 (Fig.5) are clearly identified as BWP (Family A, Table1), with their high iron content (30-
359 40 wt% normalized without C and O). The detection of minor elements such as Cu, Zn, Ba, Mn, and
360 Cr, which are considered tracers of brake emissions as observed in BWP (Figure 3), is also salient in
361 the submicron fraction. Moreover, they have no internal mixture with road salt (Na, and N or Cl) so
362 they can be considered as freshly emitted BWP, in contrast to particles from Family B containing road
363 salt. In fact, with the exception of particles from Family A, all TRCP contain road salts (i.e., Na and
364 Cl or N) and are shown to be contaminated with RRD. If the relative abundance of the main tracers of
365 RRD (Na and Cl) differs from one cluster to another (0.1 to 10 wt.% - Fig.5), particles contaminated
366 with RRD count for 79% of TRCP in the micron fraction and 88% in the submicron fraction. During
367 icy periods, the salt spread on the road consists of sodium chloride (NaCl), which is prone to
368 undergoing compositional changes over time due to the influence of anthropogenic gaseous species,
369 such as sea salt particles during their aging process (Adachi and Buseck, 2015). In anthropogenic

370 environment, the aged salt particles often undergo internal mixing with sulfate and nitrate (Hara et al.,
371 2005), frequently resulting in significant chloride depletion (Laskin et al., 2012). The presence of NO_x
372 in urban environments is undeniable, leading to the partial conversion of NaCl into NaNO₃, which
373 explains the frequent presence of nitrogen associated with sodium in RRD. However, this does not
374 provide any information about their emission process. These particles could be road dust that has been
375 resuspended due to turbulences caused by vehicle movement, or they may originate from road dust
376 previously incrustated in the tire surface, subsequently crushed, and ejected during the tire-road contact.
377 This assumption is based on the presence of major elements characteristic of TWP (as C, Si, Al, Fe, S,
378 and Zn) in four out of the nine Families (Table 1, Families C, D, E and F), combined with RRD in all
379 cases. Finally, road wear particles (RWP) composed of Ca-Fe-rich particles, along with Si, Al, S, Mg,
380 P, and K to a lesser extent, may also be contaminated by road salt (family G in our classification –
381 Table 1).

382 In conclusion, while the chemical composition of particles greatly differs according to the size fraction,
383 this study confirms the importance of road dust as a source of TRCP and demonstrates that in the real
384 environment and at the scale of the individual particle, no TRCP is derived solely from tire or road
385 source materials. Indeed, all TWP and RWP are internal mixtures with road dust and it is difficult to
386 distinguish RRD from TWP, RWP and/or BWP because TRCP are always contaminated by road dust.
387 Moreover, the high contribution of these agglomerated particles in the submicron fraction indicates
388 that a significant fraction of the TRCP resulting from RRD are submicronic particles.

389 Micron and submicron TRCP emissions in the absence of road salting: An additional experiment was
390 performed the day after the on-road measurements on a pre-cleaned test track to reduce the contribution
391 of road dust to TRCP emissions as much as possible. The TRCP collected exhibited the same various
392 morphologies, e.g., spherical, agglomerated or elongated (data not reported here), as particles sampled
393 during the on-road experiment. As expected, the contribution of road salts to TRCP is significantly
394 lower than for the on-road measurements (Figure 6). As a consequence, no contribution of road dust

395 was observed in BWP emissions (Table 1, right column, Families A and B). The contribution of
396 clusters containing RRD from road salting to agglomerated brake-, tire- and road-wear particles fell
397 from 87 to 60% (Family C) and from 39 to 26% (Family D), which is expected considering the low
398 road surface dustiness of the pre-cleaned test track compared to the road. The contribution of road dust
399 is only discernable for particles identified as TWP (Family F, Table 1) and RWP (Family G), but the
400 related clusters proportion correspond to < 10% of analyzed particles. The only exception is the
401 residual presence of RRD from road salting in particles likely coming from tire rubber abrasion
402 (Family E), which represent 43% of submicron TRCP analyzed. Thus, we assume that, despite the
403 washing of the road surface before the test-track measurements, these remaining road salts probably
404 come from aged particles previously encrusted at the surface of the tire tread during the earlier on-road
405 experiment and ejected during the test-track measurements carried out the next day. The absence of
406 road salts in collected BWP confirms this hypothesis. Therefore, when measuring/quantifying TWP in
407 real-environment, it is essential to consider the re-emission phenomenon of road dust.

408

409 **4. Conclusion**

410 The aim of the present study was to develop an original experimental approach that offers insights into
411 the chemical composition of TRCP emissions and to explore the diverse origins of TRCP, linked to
412 the source materials (tire, road surface, brake system, etc.). Super-coarse TRCP can be classified into
413 three categories: carbon- and metal-rich TWP, high-mineral content RWP, and agglomerated particles
414 including RRD. The measurements in real-driving conditions have allowed us to demonstrate the
415 significant contribution of road dust to the micron and submicron fractions of TRCP emissions (79%
416 and 88% of particles, respectively). Moreover, on an individual particle scale, TRCP are consistently
417 associated with road dust compounds, and it is rare to find TWP or RWP composed solely of tire or
418 road materials, respectively. BWP contribution to TRCP is characterized by the emission of Fe-rich
419 particles, including related heavy metals like Ba and/or Mn. In addition to rubber abrasion producing

420 C-rich particles, TWP present in TRCP are made up of an abundance of Si and Zn from the filler
421 mixture of the tire tread, as well as S, acting as a rubber vulcanization agent. Apart from the presence
422 of compounds from road dust, RWP are distinguished by their high-mineral content, primarily
423 comprising Ca and Fe, along with smaller amounts of Si, Al, S, Mg, P, and K. Complementary
424 measurements on a pre-cleaned test track have shown that road dust contamination to TRCP emission
425 might be from aged particles incrustated at the surface of the tire and re-emitted by friction with the road
426 surface.

427 Our study highlights the challenge of accurately characterizing TRCP emitted in a real environment,
428 disregarding the particles previously deposited on the road surface, as their nature and quantity are
429 independent of the characteristics of the vehicle tested. For this reason, we recommend that future
430 studies aiming to gain a better understanding of the particles emitted at the tire-road contact should
431 systematically characterize both the dustiness and the road surface (roughness) simultaneously. While
432 challenging to achieve under driving conditions, the use of an on-board high-frequency image
433 acquisition camera combined with an intelligent recognition system should make it possible to
434 correlate TRCP emissions with the specific characteristics of the roadway (roughness and dust
435 emission). Nevertheless, experiments on test tracks in a controlled environment seem to be essential
436 for a more accurate assessment of wear particles from vehicles alone.

437 **5. Acknowledgements**

438 This study was funded by ADEME (French Environment and Energy Management Agency) through
439 the “Physical Characterization of the Non-Exhaust Particle Emissions by Road Vehicles” project (or
440 Captatus) (grant number: 1566C0016). In particular, the authors would like to acknowledge L.
441 Gagnepain with ADEME for fruitful scientific exchanges and thank L. Suard, S. Louis, A. Guilloux
442 and S. Buisson for their assistance in setting up the test track experiments and ensuring vehicle
443 availability.

444 The work was partially supported by the French Ministère de l'Enseignement Supérieur, de la Recherche
445 et de l'Innovation, the region Hauts-de-France and the European Regional Development Fund (CPER
446 research projects IREN and Ecrin). LPCA is part of the CaPPA (Chemical and Physical Properties of
447 the Atmosphere) Labex funded by the French National Research Agency (ANR) through the PIA
448 (Programme d'Investissement d'Avenir; contract no. ANR-11-LABX-0005-01) and by the regional
449 council of Hauts-de-France and the European Regional Development Fund.

450

451

6. References

452 Adachi, K., Buseck, P.R., 2015. Changes in shape and composition of sea-salt particles upon aging in
453 an urban atmosphere. *Atmos. Environ.* 100, 1–9. <https://doi.org/10.1016/j.atmosenv.2014.10.036>

454 Adachi, K., Tainosho, Y., 2004. Characterization of heavy metal particles embedded in tire dust.
455 *Environ. Int.* 30, 1009–1017. <https://doi.org/10.1016/j.envint.2004.04.004>

456 Alves, C.A., Vicente, A.M.P., Calvo, A.I., Baumgardner, D., Amato, F., Querol, X., Pio, C.,
457 Gustafsson, M., 2020. Physical and chemical properties of non-exhaust particles generated from wear
458 between pavements and tyres. *Atmos. Environ.* 224, 117252.
459 <https://doi.org/10.1016/j.atmosenv.2019.117252>

460 Baensch-Baltruschat, B., Kocher, B., Stock, F., Reifferscheid, G., 2020. Tyre and road wear particles
461 (TRWP) - A review of generation, properties, emissions, human health risk, ecotoxicity, and fate in
462 the environment. *Sci. Total Environ.* 733, 137823. <https://doi.org/10.1016/j.scitotenv.2020.137823>

463 Beji, A., Deboudt, K., Khardi, S., Muresan, B., Flament, P., Fourmentin, M., Lumière, L., 2020. Non-
464 exhaust particle emissions under various driving conditions: Implications for sustainable mobility.
465 *Transp. Res. Part Transp. Environ.* 81, 102290. <https://doi.org/10.1016/j.trd.2020.102290>

466 Beji, A., Deboudt, K., Khardi, S., Muresan, B., Lumière, L., 2021. Determinants of rear-of-wheel and
467 tire-road wear particle emissions by light-duty vehicles using on-road and test track experiments.
468 *Atmospheric Pollut. Res.* 12, 278–291. <https://doi.org/10.1016/j.apr.2020.12.014>

469 Camatini, M., Crosta, G.F., Dolukhanyan, T., Sung, C., Giuliani, G., Corbetta, G.M., Cencetti, S.,
470 Regazzoni, C., 2001. Microcharacterization and identification of tire debris in heterogeneous
471 laboratory and environmental specimens. *Mater. Character.* 46, 271–283. <https://doi.org/10.1016/S1044->
472 5803(00)00098-X

473 Candeias, C., Vicente, E., Tomé, M., Rocha, F., Ávila, P., Céilia, A., 2020. Geochemical, Mineralogical
474 and Morphological Characterisation of Road Dust and Associated Health Risks. *Int. J. Environ. Res.*
475 *Public. Health* 17, 1563. <https://doi.org/10.3390/ijerph17051563>

476 Cao, J., Huang, H., Jiao, R., Pei, J., Xu, Y., RuiRen, Wang, Y., 2022. The study of wear particle
477 emissions of soft rubber on rolling contact under braking conditions. *Wear* 506–507, 204431.
478 <https://doi.org/10.1016/j.wear.2022.204431>

479 Celo, V., Yassine, M.M., Dabek-Zlotorzynska, E., 2021. Insights into Elemental Composition and
480 Sources of Fine and Coarse Particulate Matter in Dense Traffic Areas in Toronto and Vancouver,
481 Canada. *Toxics* 9, 264. <https://doi.org/10.3390/toxics9100264>

482 Charron, A., Polo-Rehn, L., Besombes, J.-L., Golly, B., Buisson, C., Chanut, H., Marchand, N.,
483 Guillaud, G., Jaffrezo, J.-L., 2019. Identification and quantification of particulate tracers of exhaust
484 and non-exhaust vehicle emissions. *Atmospheric Chem. Phys.* 19, 5187–5207.
485 <https://doi.org/10.5194/acp-19-5187-2019>

486 Chen, Y., Xu, S., Tebaldi, G., Romeo, E., 2022. Role of mineral filler in asphalt mixture. *Road Mater.*
487 *Pavement Des.* 23, 247–286. <https://doi.org/10.1080/14680629.2020.1826351>

488 Chousidis, N., Ioannou, I., Rakanta, E., Koutsodontis, C., Batis, G., 2016. Effect of fly ash chemical
489 composition on the reinforcement corrosion, thermal diffusion and strength of blended cement
490 concretes. *Constr. Build. Mater.* 126, 86–97. <https://doi.org/10.1016/j.conbuildmat.2016.09.024>

491 Cunha-Lopes, I., Alves, C.A., Casotti Rienda, I., Faria, T., Lucarelli, F., Querol, X., Amato, F.,
492 Almeida, S.M., 2022. Characterisation of non-exhaust emissions from road traffic in Lisbon. *Atmos.*
493 *Environ.* 286, 119221. <https://doi.org/10.1016/j.atmosenv.2022.119221>

494 Deng, Y., Hu, M., Xu, L., Ling, S., Ni, H., Sun, D., 2022. Dual roles played by manganese dioxide
495 filler in asphalt pavement material: Chemical modification and healing improvement. *Constr. Build.*
496 *Mater.* 345, 128371. <https://doi.org/10.1016/j.conbuildmat.2022.128371>

497 Eisentraut, P., Dümichen, E., Ruhl, A.S., Jekel, M., Albrecht, M., Gehde, M., Braun, U., 2018. Two
498 Birds with One Stone—Fast and Simultaneous Analysis of Microplastics: Microparticles Derived from
499 Thermoplastics and Tire Wear. *Environ. Sci. Technol. Lett.* 5, 608–613.
500 <https://doi.org/10.1021/acs.estlett.8b00446>

501 Fussell, J.C., Franklin, M., Green, D.C., Gustafsson, M., Harrison, R.M., Hicks, W., Kelly, F.J., Kishta,
502 F., Miller, M.R., Mudway, I.S., Oroumihyeh, F., Selley, L., Wang, M., Zhu, Y., 2022. A Review of

503 Road Traffic-Derived Non-Exhaust Particles: Emissions, Physicochemical Characteristics, Health
504 Risks, and Mitigation Measures. *Environ. Sci. Technol.* 56, 6813–6835.
505 <https://doi.org/10.1021/acs.est.2c01072>

506 Gao, Z., Cizdziel, J.V., Wontor, K., Clisham, C., Focia, K., Rausch, J., Jaramillo-Vogel, D., 2022. On
507 airborne tire wear particles along roads with different traffic characteristics using passive sampling
508 and optical microscopy, single particle SEM/EDX, and μ -ATR-FTIR analyses. *Front. Environ. Sci.*
509 10.

510 Gomes Nogueira, A.P., Carlevaris, D., Menapace, C., Straffelini, G., 2020. Tribological and Emission
511 Behavior of Novel Friction Materials. *Atmosphere* 11, 1050. <https://doi.org/10.3390/atmos11101050>

512 Gunawardana, C., Goonetilleke, A., Egodawatta, P., Dawes, L., Kokot, S., 2012. Source
513 characterisation of road dust based on chemical and mineralogical composition. *Chemosphere* 87,
514 163–170. <https://doi.org/10.1016/j.chemosphere.2011.12.012>

515 Gustafsson, M., 2018. Review of Road Wear Emissions, in: *Non-Exhaust Emissions*. Elsevier, pp.
516 161–181. <https://doi.org/10.1016/B978-0-12-811770-5.00008-X>

517 Halle, L.L., Palmqvist, A., Kampmann, K., Khan, F.R., 2020. Ecotoxicology of micronized tire rubber:
518 Past, present and future considerations. *Sci. Total Environ.* 706, 135694.
519 <https://doi.org/10.1016/j.scitotenv.2019.135694>

520 Hara, K., Osada, K., Kido, M., Matsunaga, K., Iwasaka, Y., Hashida, G., Yamanouchi, T., 2005.
521 Variations of constituents of individual sea-salt particles at Syowa station, Antarctica. *Tellus B Chem.*
522 *Phys. Meteorol.* 57, 230. <https://doi.org/10.3402/tellusb.v57i3.16530>

523 Harrison, R.M., Allan, J., Carruthers, D., Heal, M.R., Lewis, A.C., Marnier, B., Murrells, T., Williams,
524 A., 2021. Non-exhaust vehicle emissions of particulate matter and VOC from road traffic: A review.
525 *Atmos. Environ.* 262, 118592. <https://doi.org/10.1016/j.atmosenv.2021.118592>

526 Järllskog, I., Jaramillo-Vogel, D., Rausch, J., Perseguers, S., Gustafsson, M., Strömvall, A.-M.,
527 Andersson-Sköld, Y., 2022. Differentiating and Quantifying Carbonaceous (Tire, Bitumen, and Road
528 Marking Wear) and Non-carbonaceous (Metals, Minerals, and Glass Beads) Non-exhaust Particles in
529 Road Dust Samples from a Traffic Environment. *Water. Air. Soil Pollut.* 233, 375.
530 <https://doi.org/10.1007/s11270-022-05847-8>

531 Kim, G., Lee, S., 2018. Characteristics of Tire Wear Particles Generated by a Tire Simulator under
532 Various Driving Conditions. *Environ. Sci. Technol.* 52, 12153–12161.
533 <https://doi.org/10.1021/acs.est.8b03459>

534 Kim, T., Ley, M.T., Kang, S., Davis, J.M., Kim, S., Amrollahi, P., 2020. Using particle composition
535 of fly ash to predict concrete strength and electrical resistivity. *Cem. Concr. Compos.* 107, 103493.
536 <https://doi.org/10.1016/j.cemconcomp.2019.103493>

537 Knight, L.J., Parker-Jurd, F.N.F., Al-Sid-Cheikh, M., Thompson, R.C., 2020. Tyre wear particles: an
538 abundant yet widely unreported microplastic? *Environ. Sci. Pollut. Res.* 27, 18345–18354.
539 <https://doi.org/10.1007/s11356-020-08187-4>

540 Kovoichich, M., Liong, M., Parker, J.A., Oh, S.C., Lee, J.P., Xi, L., Kreider, M.L., Unice, K.M., 2021.
541 Chemical mapping of tire and road wear particles for single particle analysis. *Sci. Total Environ.* 757,
542 144085. <https://doi.org/10.1016/j.scitotenv.2020.144085>

543 Kreider, M.L., Panko, J.M., McAtee, B.L., Sweet, L.I., Finley, B.L., 2010. Physical and chemical
544 characterization of tire-related particles: Comparison of particles generated using different
545 methodologies. *Sci. Total Environ.* 408, 652–659. <https://doi.org/10.1016/j.scitotenv.2009.10.016>

546 Kreider, M.L., Unice, K.M., Panko, J.M., 2020. Human health risk assessment of Tire and Road Wear
547 Particles (TRWP) in air. *Hum. Ecol. Risk Assess. Int. J.* 26, 2567–2585.
548 <https://doi.org/10.1080/10807039.2019.1674633>

549 Kukutschová, J., Roubíček, V., Malachová, K., Pavlíčková, Z., Holuša, R., Kubačková, J., Mička, V.,
550 MacCrimmon, D., Filip, P., 2009. Wear mechanism in automotive brake materials, wear debris and its
551 potential environmental impact. *Wear* 267, 807–817. <https://doi.org/10.1016/j.wear.2009.01.034>

552 Laskin, A., Moffet, R.C., Gilles, M.K., Fast, J.D., Zaveri, R.A., Wang, B., Nigge, P., Shutthanandan,
553 J., 2012. Tropospheric chemistry of internally mixed sea salt and organic particles: Surprising
554 reactivity of NaCl with weak organic acids: MIXED SEA SALT/ORGANICS PARTICLES. *J.*
555 *Geophys. Res. Atmospheres* 117, n/a-n/a. <https://doi.org/10.1029/2012JD017743>

556 Mathissen, Marcel, Volker Scheer, Rainer Vogt, and Thorsten Benter, 2011. Investigation on the
557 Potential Generation of Ultrafine Particles from the Tire–Road Interface. *Atmospheric Environment*
558 45(34): 6172-79. <https://doi.org/10.1016/j.atmosenv.2011.08.032>.

559 Matthaios, V.N., Lawrence, J., Martins, M.A.G., Ferguson, S.T., Wolfson, J.M., Harrison, R.M.,
560 Koutrakis, P., 2022. Quantifying factors affecting contributions of roadway exhaust and non-exhaust

561 emissions to ambient PM_{10-2.5} and PM_{2.5-0.2} particles. *Sci. Total Environ.* 835, 155368.
562 <https://doi.org/10.1016/j.scitotenv.2022.155368>

563 Mattonai, M., Nacci, T., Modugno, F., 2022. Analytical strategies for the quali-quantitation of tire and
564 road wear particles – A critical review. *TrAC Trends Anal. Chem.* 154, 116650.
565 <https://doi.org/10.1016/j.trac.2022.116650>

566 Mistry, R., Roy, T.K., 2016. Effect of using fly ash as alternative filler in hot mix asphalt. *Perspect.*
567 *Sci.* 8, 307–309. <https://doi.org/10.1016/j.pisc.2016.04.061>

568 Padoan, E., Romè, C., Ajmone-Marsan, F., 2017. Bioaccessibility and size distribution of metals in
569 road dust and roadside soils along a peri-urban transect. *Sci. Total Environ.* 601–602, 89–98.
570 <https://doi.org/10.1016/j.scitotenv.2017.05.180>

571 Park, I., Kim, H., Lee, S., 2018. Characteristics of tire wear particles generated in a laboratory
572 simulation of tire/road contact conditions. *J. Aerosol Sci.* 124, 30–40.
573 <https://doi.org/10.1016/j.jaerosci.2018.07.005>

574 Park, I., Lee, J., Lee, S., 2017. Laboratory study of the generation of nanoparticles from tire tread.
575 *Aerosol Sci. Technol.* 51, 188–197. <https://doi.org/10.1080/02786826.2016.1248757>

576 Piscitello, A., Bianco, C., Casasso, A., Sethi, R., 2021. Non-exhaust traffic emissions: Sources,
577 characterization, and mitigation measures. *Sci. Total Environ.* 766, 144440.
578 <https://doi.org/10.1016/j.scitotenv.2020.144440>

579 Rattanasom, N., Saowapark, T., Deeprasertkul, C., 2007. Reinforcement of natural rubber with
580 silica/carbon black hybrid filler. *Polym. Test.* 26, 369–377.
581 <https://doi.org/10.1016/j.polymertesting.2006.12.003>

582 Rausch, J., Jaramillo-Vogel, D., Perseguers, S., Schnidrig, N., Grobéty, B., Yajan, P., 2022. Automated
583 identification and quantification of tire wear particles (TWP) in airborne dust: SEM/EDX single
584 particle analysis coupled to a machine learning classifier. *Sci. Total Environ.* 803, 149832.
585 <https://doi.org/10.1016/j.scitotenv.2021.149832>

586 Sanders, P.G., Xu, N., Dalka, T.M., Maricq, M.M., 2003. Airborne Brake Wear Debris: Size
587 Distributions, Composition, and a Comparison of Dynamometer and Vehicle Tests. *Environ. Sci.*
588 *Technol.* 37, 4060–4069. <https://doi.org/10.1021/es034145s>

589 Sommer, F., Dietze, V., Baum, A., Sauer, J., Gilge, S., Maschowski, C., Gieré, R., 2018. Tire Abrasion
590 as a Major Source of Microplastics in the Environment. *Aerosol Air Qual. Res.* 18, 2014–2028.
591 <https://doi.org/10.4209/aaqr.2018.03.0099>

592 Wagner, S., Hüffer, T., Klöckner, P., Wehrhahn, M., Hofmann, T., Reemtsma, T., 2018. Tire wear
593 particles in the aquatic environment - A review on generation, analysis, occurrence, fate and effects.
594 *Water Res.* 139, 83–100. <https://doi.org/10.1016/j.watres.2018.03.051>

595 Wei, M., Wu, S., Xu, H., Li, H., Yang, C., 2021. Characterization of Steel Slag Filler and Its Effect on
596 Aging Resistance of Asphalt Mastic with Various Aging Methods. *Materials* 14, 869.
597 <https://doi.org/10.3390/ma14040869>

598 Xu, G., Shi, X., 2018. Characteristics and applications of fly ash as a sustainable construction material:
599 A state-of-the-art review. *Resour. Conserv. Recycl.* 136, 95–109.
600 <https://doi.org/10.1016/j.resconrec.2018.04.010>

601 Yan, H., Zhang, L., Liu, L., Wen, S., 2021. Investigation of the external conditions and material
602 compositions affecting the formation mechanism and size distribution of tire wear particles. *Atmos.*
603 *Environ.* 244, 118018. <https://doi.org/10.1016/j.atmosenv.2020.118018>

604 Yang, Y., Vance, M., Tou, F., Tiwari, A., Liu, M., Hochella, M.F., 2016. Nanoparticles in road dust
605 from impervious urban surfaces: distribution, identification, and environmental implications. *Environ.*
606 *Sci. Nano* 3, 534–544. <https://doi.org/10.1039/C6EN00056H>

607 Youn, J.-S., Kim, Y.-M., Siddiqui, M.Z., Watanabe, A., Han, S., Jeong, S., Jung, Y.-W., Jeon, K.-J.,
608 2021. Quantification of tire wear particles in road dust from industrial and residential areas in Seoul,
609 Korea. *Sci. Total Environ.* 784, 147177. <https://doi.org/10.1016/j.scitotenv.2021.147177>

610 Zhang, J., Peng, J., Song, C., Ma, C., Men, Z., Wu, J., Wu, L., Wang, T., Zhang, X., Tao, S., Gao, S.,
611 Hopke, P.K., Mao, H., 2020. Vehicular non-exhaust particulate emissions in Chinese megacities:
612 Source profiles, real-world emission factors, and inventories. *Environ. Pollut.* 266, 115268.
613 <https://doi.org/10.1016/j.envpol.2020.115268>

614 Zhang, M., Yin, H., Tan, J., Wang, X., Yang, Z., Hao, L., Du, T., Niu, Z., Ge, Y., 2023. A
615 comprehensive review of tyre wear particles: Formation, measurements, properties, and influencing
616 factors. *Atmos. Environ.* 297, 119597. <https://doi.org/10.1016/j.atmosenv.2023.119597>

617

618

619 **List of Table**

Family	Major elements detected in individual particles by EDX analysis	Probable origin	“On-road” (R-) clusters	“On test track” (T-) clusters
A	Fe-rich	Fresh-BWP	R-TRCP-M3 (21%) R-TRCP-S2 (12%)	T-TRCP-M3 (20%) T-TRCP-S2 (29%)
B	Fe-rich and other heavy metals (with Na, N/Cl)	BWP (and RRD from road salting)	R-TRCP-M2 (32%) R-TRCP-M5 (2%)	-
C	C-rich and Si, Al, Fe (with Na, N/Cl)	Agglomerated BWP + RWP + TWP (and RRD from road salting)	R-TRCP-S1 (80%) R-TRCP-S4 (3%) R-TRCP-M4 (4%)	T-TRCP-M2 (26%) T-TRCP-M4 (17%) T-TRCP-S3 (17%)
D	C-rich and Fe (with Na, Cl)	Agglomerated BWP + RWP + TWP (and RRD from road salting)	R-TRCP-M1 (39%)	T-TRCP-M1 (26%)
E	C-rich (with Na, Cl)	TWP (rubber tread abrasion) (and RRD from road salting)	R-TRCP-S3 (5%)	T-TRCP-S1 (43%)
F	C-rich and Si, S, Zn (with Na, Cl)	TWP (and RRD from road salting)	-	T-TRCP-M5 (9%) T-TRCP-S5 (4%)
G	Ca-Fe-rich and Al, Si, Mg, S, P, K (with Na, Cl)	RWP (and RRD from road salting)	R-TRCP-M6 (1%)	T-TRCP-M6 (3%) T-TRCP-S4 (5%)

620
621
622
623

Table 1 : Overview of the different TRCP families and their probable origins. The assignment of particles from the micron (TRCP-M) and the submicron (TRCP-S) fractions collected during “on-road” (R-) and on “test track” (T-) experiments is reported in the two last columns respectively, with their relative contribution (%) in parentheses.

624 **Figure Captions**

625

626 **Figure 1:** Schematic view of Non-Exhaust Particles (NEP) emissions.

627 **Figure 2:** Illustrations (upper and lower panels) and schematic view (middle panel) of the
628 instrumental set-up implemented to monitor particulate emissions from the tire-road interface. The
629 orientation and velocity of streamlines were calculated at stabilized driving speeds using
630 Computational Fluid Dynamics (CFD) modeling with the Ansys Fluent application. The red coloring
631 represents the highest velocities. (*Reprinted from Beji et al., 2021 – Courtesy of Elsevier©*).
632 The black adhesive disk used for passive sampling of super-coarse particles is visible at the end of
633 the air inlet.

634 **Figure 3:** Chemical composition (in wt. %) of BWP (total analyzed particles =768), collected on-road
635 (R), for the micron (1-10 μm) and submicron (0.1-1 μm) size fractions. Numbering system used is as
636 follows: the clusters numbered # are named “R-BWP-M#” and “R-BWP-S#” for the micron (M) and
637 submicron (S) fractions, respectively. The relative contribution (RC) of each cluster is indicated below
638 the cluster name.

639 **Figure 4:** SEM pictures of super-coarse TRCP sampled during the test-track experiments with
640 different origins: a) road wear, b) and c) tire wear, d) filler mixture of tire tread, e) tire rubber, f)
641 agglomeration of particles from both tire and road wear.

642 **Figure 5:** Chemical composition (in wt. %) of TRCP (total analyzed particles =925) collected on-
643 road (R) for the micron (1-10 μm) and submicron (0.1-1 μm) size fractions. The clusters numbered #
644 are named “R-TRCP-M#” and “R-TRCP-S#” for the micron (M) and submicron (S) fractions,
645 respectively. The relative contribution (RC) of each cluster is indicated below the cluster name.

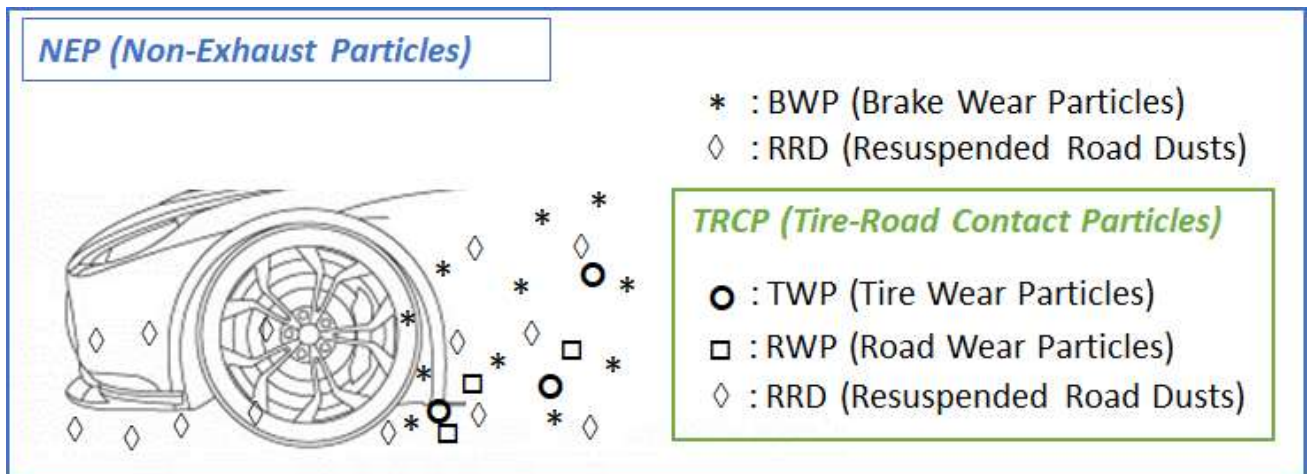
646 **Figure 6:** Chemical composition (in wt. %) of TRCP (total analyzed particles=617) collected on the
647 cleaned test track (T) for the micron (1-10 μm) and submicron (0.1-1 μm) size fractions. The clusters

648 numbered # are named T-TRCP-M# and T-TRCP-S# for the micron (M) and submicron (S)
649 fractions, respectively. The relative contribution (RC) of each cluster is indicated below the cluster.

650

651 Figure 1

652

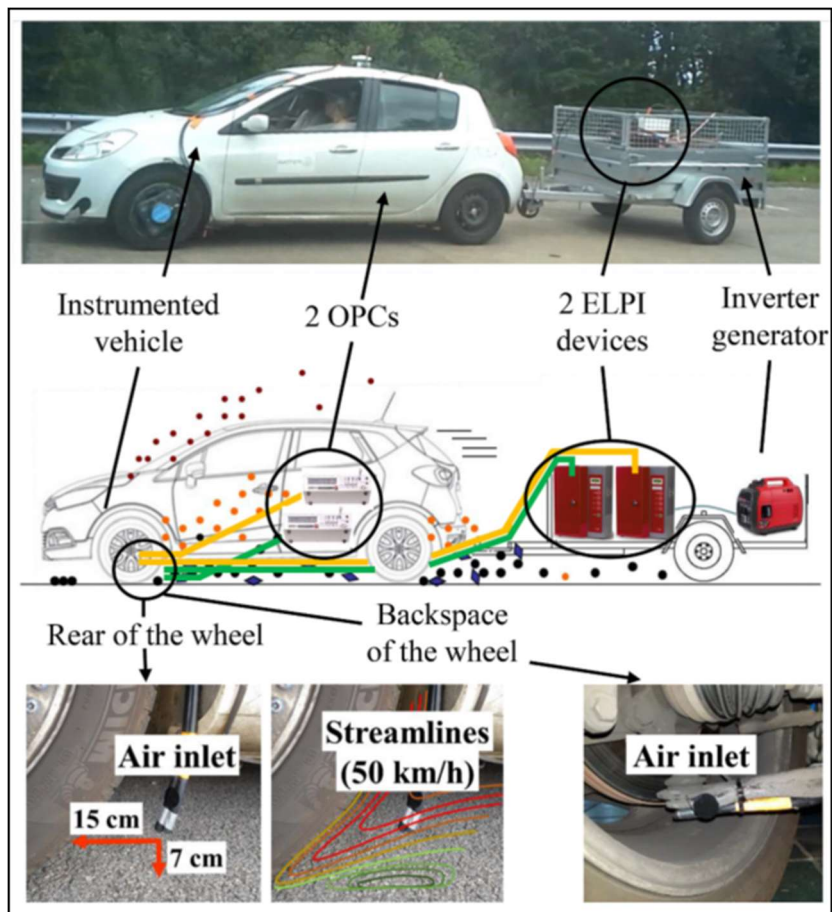


653

654

655 **Figure 2**

656

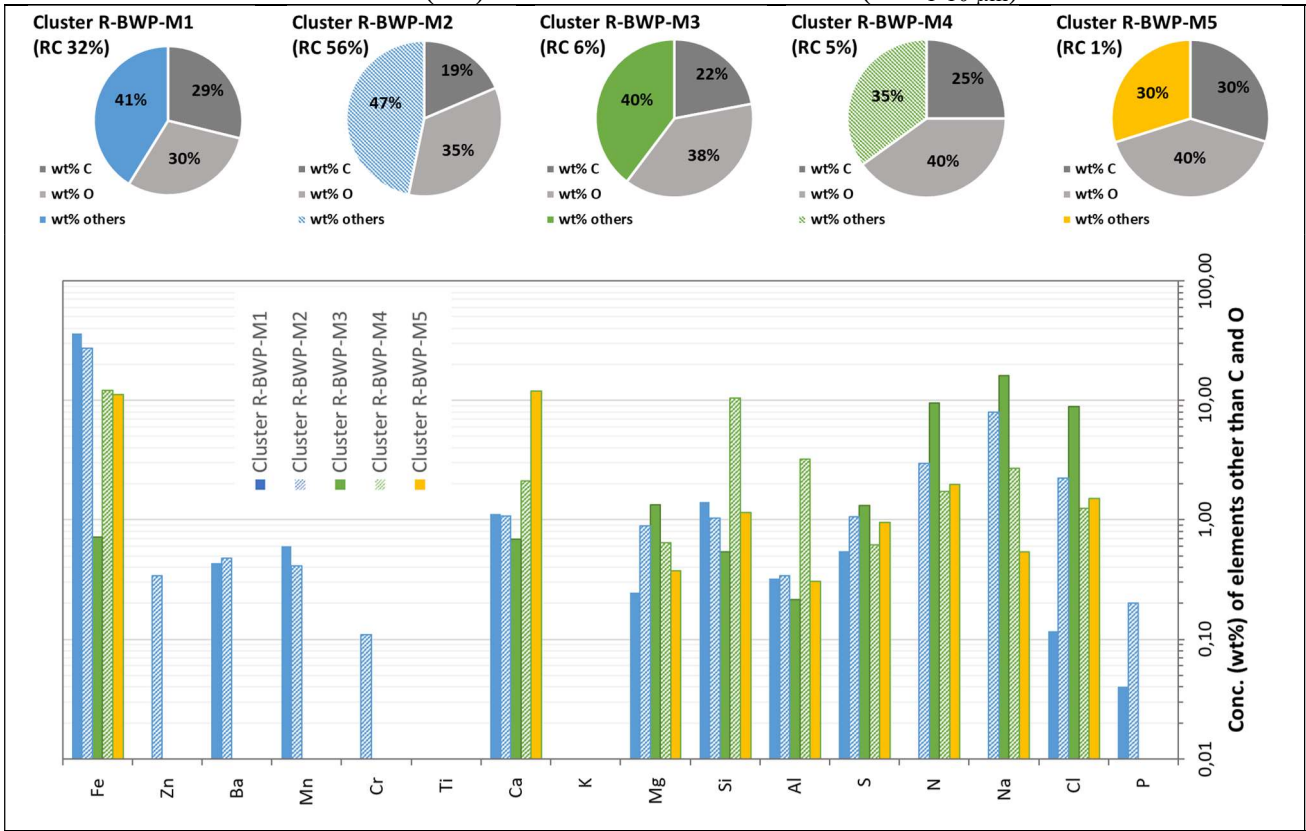


657

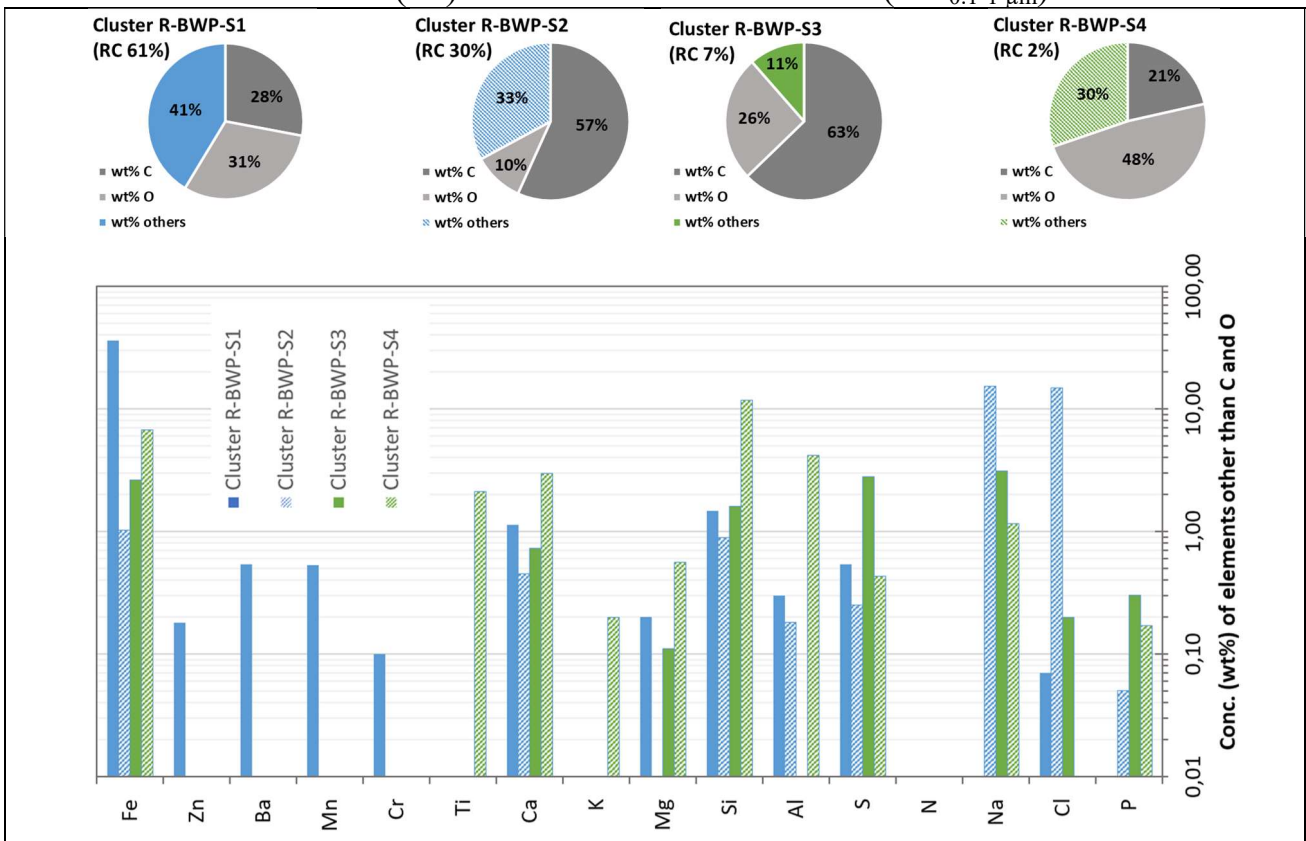
658

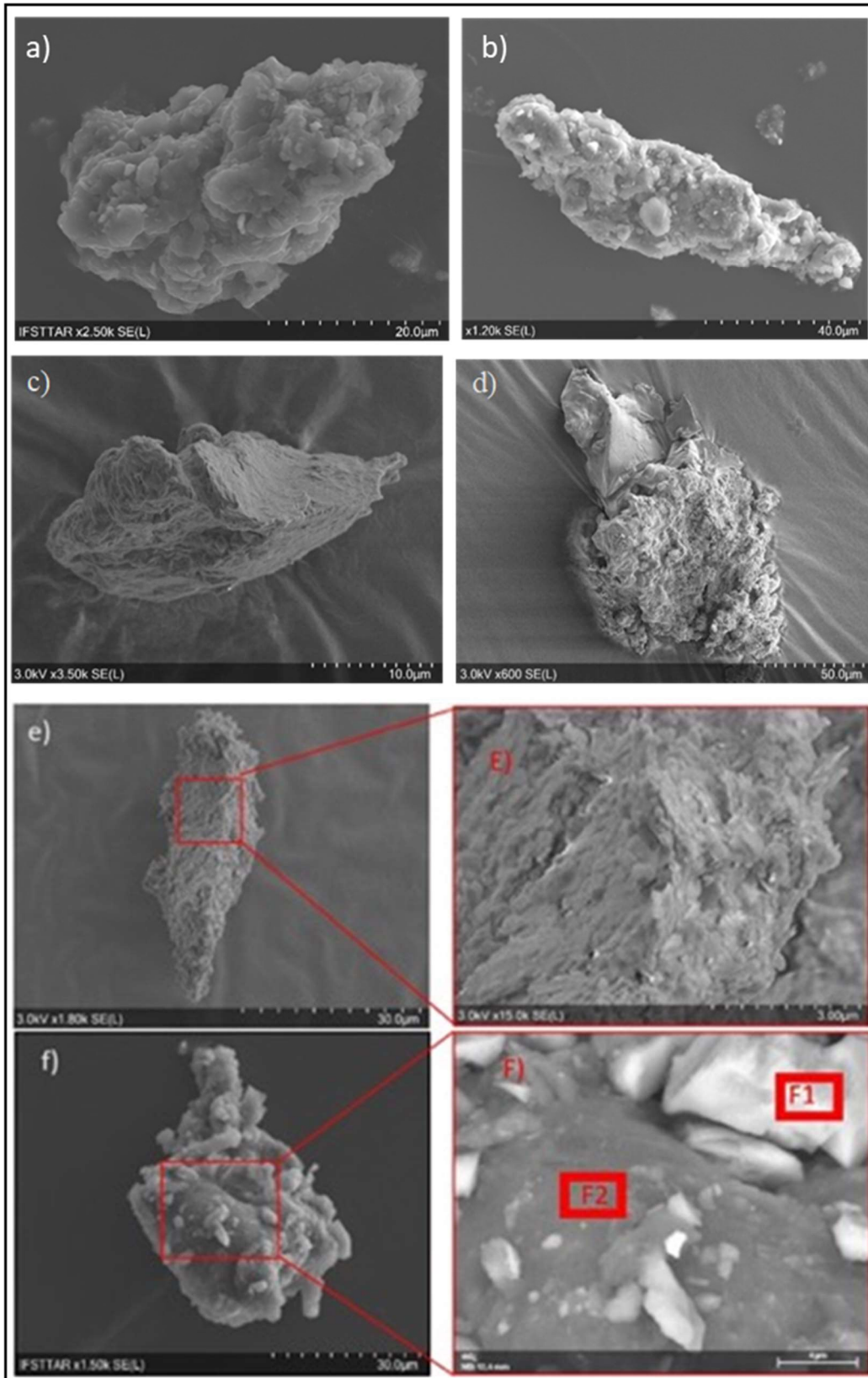
659 **Figure 3**

On-road (R-) BWP - Micron fraction (PM_{1-10 μm})



On-road (R-) BWP - Submicron fraction (PM_{0.1-1 μm})

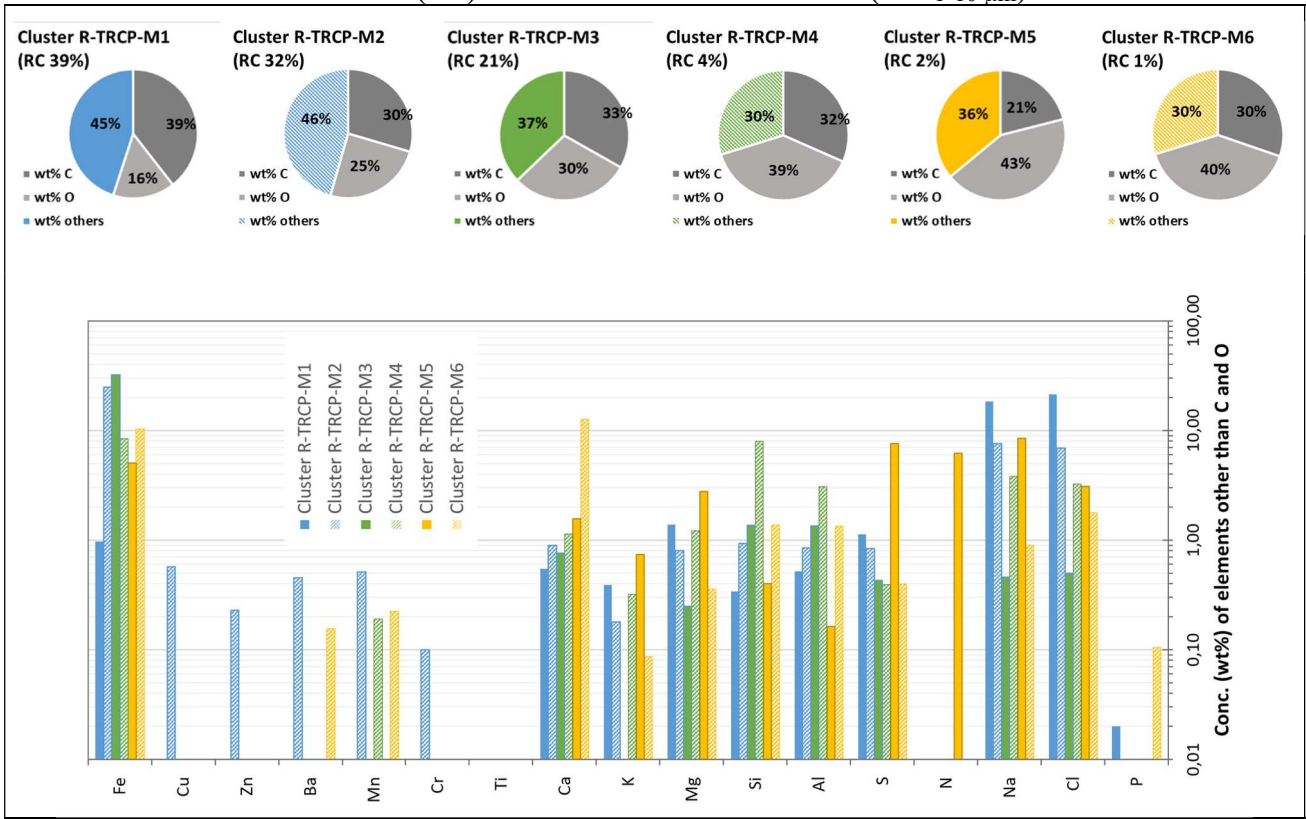




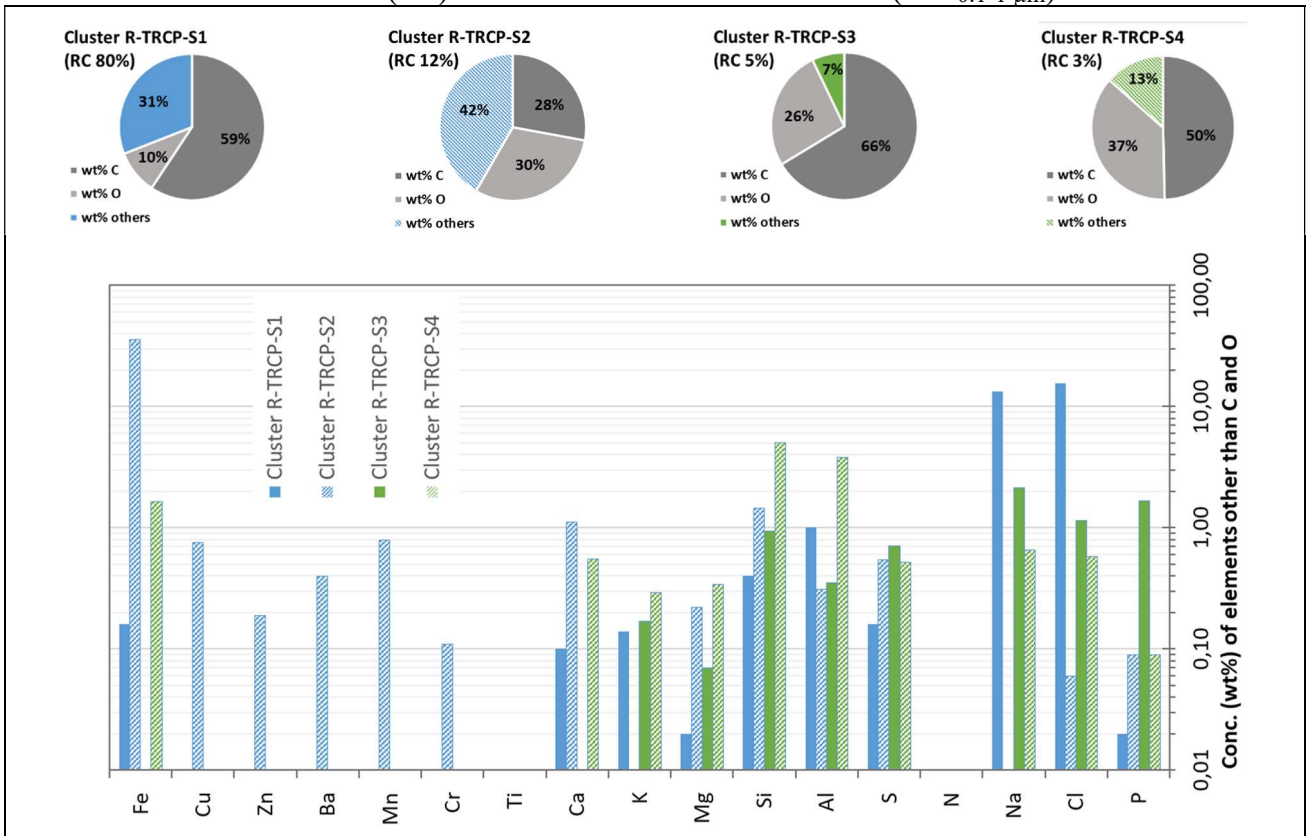
661

662

On-road (R-) TRCP - Micron fraction (PM_{1-10 μm})



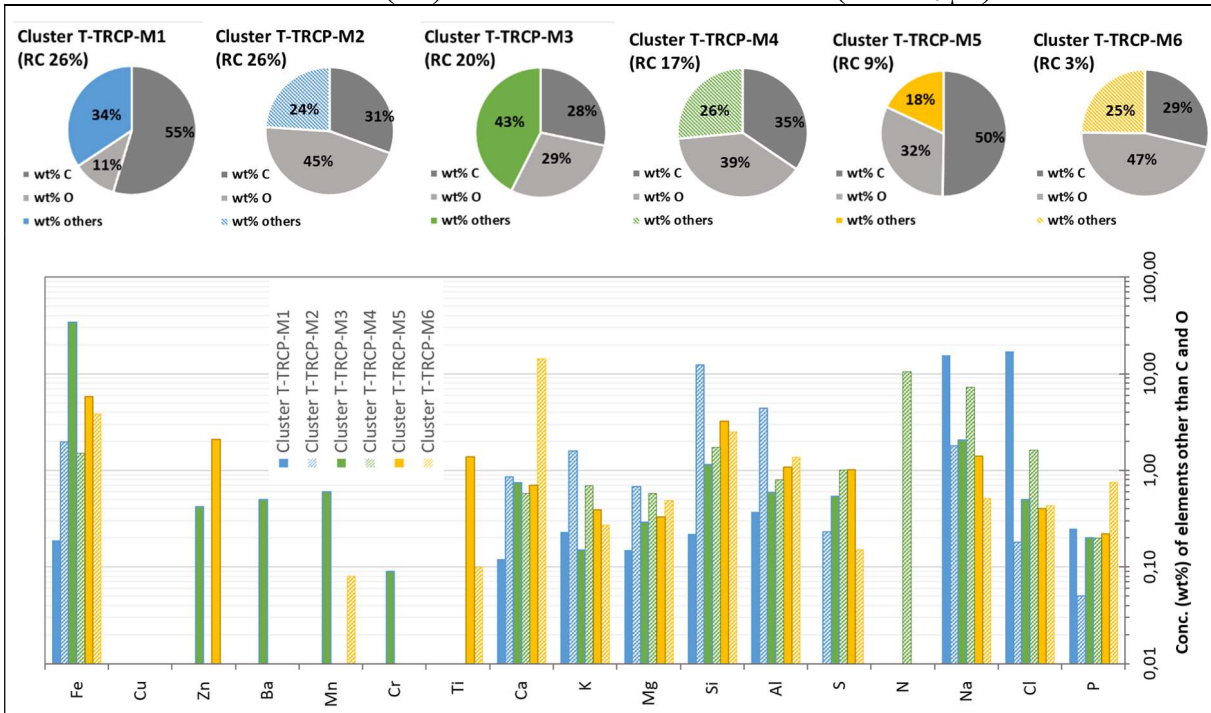
On-road (R-) TRCP - Submicron fraction (PM_{0.1-1 μm})



664 **Figure 6**

665

Test track (T-) TRCP - Micron fraction (PM₁₋₁₀ μm)



Test track (T-) TRCP - Submicron fraction (PM_{0.1-1} μm)



666

667